Refined solution structure of the oligomerization domain of the tumour suppressor p53

G. Marius Clore[1], James Ernst[1], Robert Clubb[1], James G. Omichinski[1], W.M. Poindexter Kennedy[1], Kazuyasu Sakaguchi[2], Ettore Appella[2] and Angela M. Gronenborn[1]

The NMR solution structure of the oligomerization domain of the tumour suppressor p53 (residues 319-360) has been refined. The structure comprises a dimer of dimers, oriented in an approximately orthogonal manner. The present structure determination is based on 4,472 experimental NMR restraints which represents a three and half fold increase over our previous work in the number of NOE restraints at the tetramerization interface. A comparison with the recently solved 1.7 Å resolution X-ray structure shows that the structures are very similar and that the average angular root-mean-square difference in the interhelical angles is about 1°. The results of recent extensive mutagenesis data and the possible effects of mutations which have been identified in human cancers are discussed in the light of the present structure.

[1]Laboratory of Chemical Physics, Building 5, National Institute of Diabetes and Digestive and Kidney Diseases, National Institutes of Health, Bethesda, MD 20892-0520, USA
[2]Laboratory of Cell Biology, Building 37, National Cancer Institute, National Institutes of Health, Bethesda, MD 20892, USA

Correspondence should be addressed to G.M.C. and A.M.G.

The tumour suppressor p53 is involved in approximately 50% of all human cancers[1–5]. It is composed of an amino-terminal transactivation domain, a central DNA-binding domain, an oligomerization domain and a carboxy-terminal, basic, regulatory domain[6–10]. The structure of the core domain complexed to DNA has been solved crystallographically[11] and the oligomerization domain by both NMR[12–14] and X-ray crystallography[15]. All the structures of the oligomerization domain have the same overall topology comprising of a dimer of dimers, oriented in an approximately orthogonal manner. Each dimer (comprising subunits A and C, and B and D[12]) consists of two antiparallel α-helices and an antiparallel β-sheet. The β-sheets lie on opposite sides of the tetramer and the helices form an unusual, four-helix bundle.

All structures show differences, chiefly in the orientation of the two dimers (Table 1), but also in the compactness of the tetramer (due to the small number of inter-subunit restraints in the case of the NMR structures) and the degree of bending of the individual α-helices. The original NMR structure[12], which first established the topology of the tetramer, was based on a data set in which several critical NOEs involving Leu 350 had been omitted and which contained three very weak NOE restraints between helices A and B which were subsequently discovered to be incorrect (due to stpectra atrifacts in the 4D $^{13}C/^{13}C$-separated spectrum). Recalculation from the corrected data set resulted in a structure[13] with approximately the same interhelical angles as the X-ray structure (Table 1). The backbone (N, Cα, C, O) atomic root-mean-square difference between this revised NMR structure and the X-ray structure was 1.2 Å for residues 326–54[13]. In contrast, the backbone atomic r.m.s. difference and the difference in the AB interhelical angle (which defines the dimer-dimer orientation) between the X-ray structure[15] on the one hand, and the original NMR structure[12] and the NMR structure of Lee *et al.*[14] on the other hand, are 3.3 Å and +34°, and 1.9 Å and -23°, respectively.

The discrepancies between the various structures illustrate the high degree of technical difficulty in solving the structure of this symmetrical homotetramer by NMR. There is thus a need for a more accurate and definitive NMR structure especially as an engineered p53 could form the basis for gene therapy. The design of such a protein containing a wild type DNA-binding domain and a mutated oligomerization domain that could oligomerize with itself but not the defective p53 within the cell, will necessarily depend on accurate solution coordinates for the dimer–dimer interface[14].

In this paper we present what we hope is a definitive solution structure of the oligomerization domain (residues 319-360) of p53 using multidimensional heteronuclear-filtered and -separated NMR spectroscopy. This structure is based on a sizeable increase, relative to our earlier structures[12,13], in the number of assigned NOEs between the subunits, obtained as a result of careful analysis of all the multidimensional NOE spectra previously acquired[12]. In addition direct refinement against $^{13}C\alpha$ and $^{13}C\beta$ chemical shifts[16] has resulted in an improvement in the stereochemistry of the backbone coordinates.

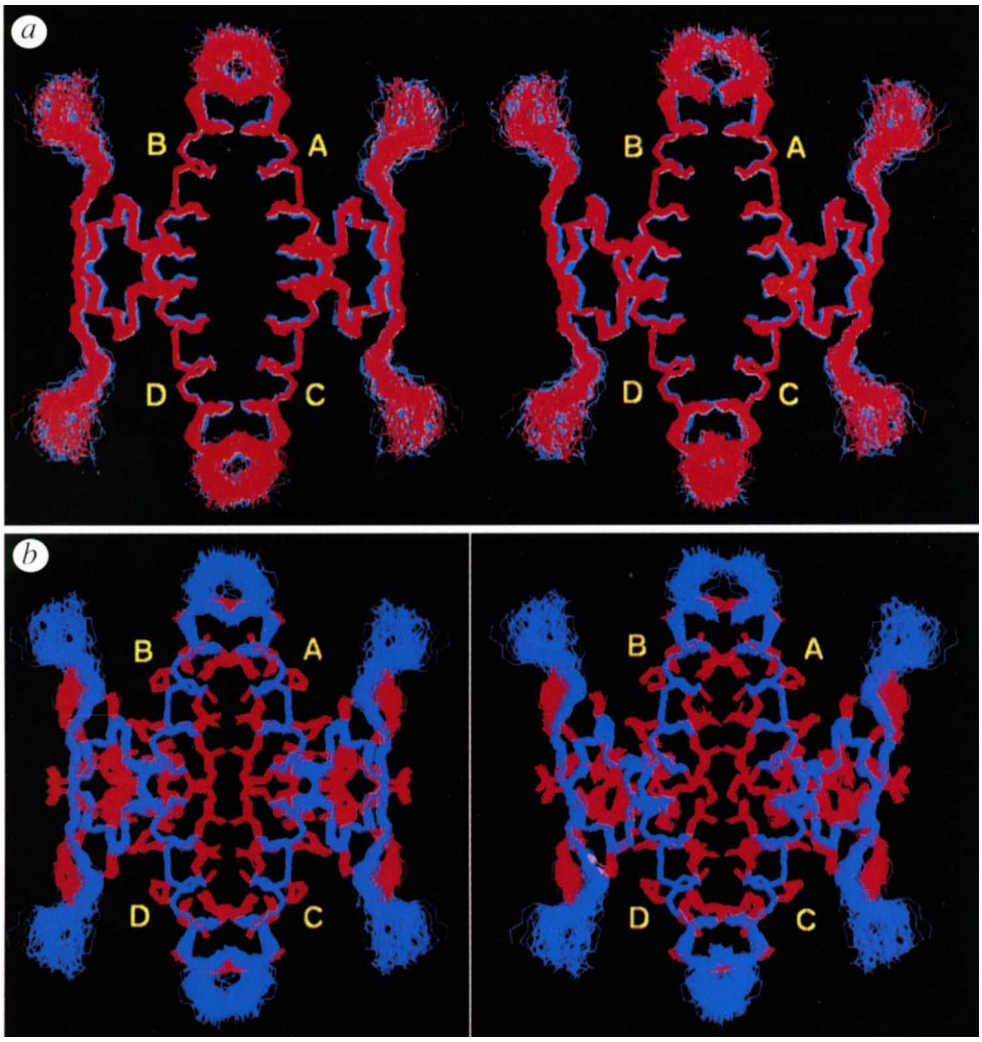

Fig. 1 *a*, Best fit superposition of the backbone (N, Cα, C) atoms of the <SA_c> (red) and <SA_d> (blue) ensemble of structures. *b*, Best fit superposition of the backbone (blue) and ordered side chains (red) of the <SA_c> ensemble of structures. Each ensemble comprises 76 structures and the backbone of residues 322–357 is displayed. The figure was generated with AVSXPLOR[54].

Structure determination

The present ensembles of simulated annealing structures are based on detailed analysis of 3D and 4D heteronuclear–separated and -filtered NOE spectra described in our original structure determination[12]. In addition 2D water selective ^{12}C-filtered H_2O-ROE-^{1}H-^{13}C, H_2O-NOE-^{1}H-^{13}C and H_2O-ROE-^{1}H-^{15}N HSQC spectra[17,18] were recorded to identify the location of bound water. The present structures are based on 4,472 experimental NMR restraints which comprise approximate interproton distance, hydrogen- bonding, torsion angle, $^3J_{HN\alpha}$ coupling constant[19], and secondary ^{13}Cα and ^{13}Cβ chemical shift[16] restraints. In addition, there are distance restraints involving four symmetrically related bound water molecules (that is one water molecule per subunit). Relative to our previous structures[12,13], the number of inter-subunit NOEs has been increased by factors of 1.2, 3.4 and 4 between the AC (BD), AB (CD) and AD (BC) subunits, respectively. This substantial increase in the number of inter-subunit NOEs, particularly at the tetramerization interface (that is between the AC and BD dimers), is the key determinant of the increase in accuracy of the present coordinates relative to our previous ones[13].

Table 1 Interhelical angles in various structures of the p53 oligomerization domain

Structure	Method	Interhelical angles (°)[1]		
		AC	AB[2]	AD
Clore *et al.* (1994)[12]	NMR	150	114	–74
Lee *et al.* (1994)[14]	NMR[3]	174	62	–117
Jeffrey & Pavletich (1995)[15]	X-ray[4]	157	80	–105
Clore *et al.* (1995)[13]	NMR[5]	154	78	–109
(SA_c)r (This work)	NMR[6]	155	81	–104
(SA_d)r (This work)	NMR[6]	154	82	–104

[1]In the notation used in this paper (as well as that in refs 12 and 13) the two primary dimers are formed by subunits A and C, and subunits B and D. The interhelical angles were calculated with the program Define_Structure[58]. The backbone (N, Cα, C, O) atomic r.m.s. differences between the X-ray structure[15] on the one hand, and the original NMR structure[12], the Lee *et al.* NMR structure[14], and our revised NMR structure[13] on the other hand, are 3.3, 1.9 and 1.2 Å, respectively, for residues 326–354.
[2]The AB angle describes the orientation of one dimer relative to the other.
[3]PDB accession code 1PES.
[4]The crystal structure was solved at a resolution of 1.7 Å and refined to an *R*-factor of 19.2 %[15].
[5]PDB Accession code 1OLG.
[6](SA_c)r and (SA_d)r are the restrained regularized mean structures derived from 76 individual simulated annealing structures calculated with the effective hard sphere van der Waals' radii derived from the CHARMM[21,22,57] and ECEPP/DISMAN/DIANA[23,24] parameters, respectively (Table 2).

Two sets of simulated annealing structures (each comprising 76 structures) were calculated (Fig. 1), employing slightly different effective hard sphere van der Waals' radii, in order to assess the uncertainties in the coordinate positions arising from the description of the non-bonded contacts[20]. These two sets of values (which are provided in Table 2 of ref. 20) represent effective radii[21] derived from the PARAM19/PARAM20 CHARMM force field[22] (giving rise to the $\langle SA_c \rangle$ ensemble of structures) and the DISMAN/DIANA radii[23] derived from the ECEPP force field[24] (giving rise to the $\langle SA_d \rangle$ ensemble of structures). As is evident from the data (Tables 2, 3), all the structures satisfy the experimental restraints within their errors while displaying very small deviations from idealized covalent geometry and good non-bonded contacts. The amino (residues 319–323) and carboxy (residues 357–360) termini are disordered, and residues 324–325, preceeding the core of the tetramer as well as residues 355–356 at the C terminus of the helix, are poorly ordered in the structures, as confirmed by ^{15}N relaxation measurements which are indicative of high mobility of backbone atoms in these regions[25]. The core of the tetramer (residues 326–354) is well defined with an overall precision in both ensembles of structures of ~ 0.3 Å for the backbone atoms, 0.7–0.8 Å for all atoms, and ~ 0.4 Å for all ordered atoms (Table 3). It should be noted,

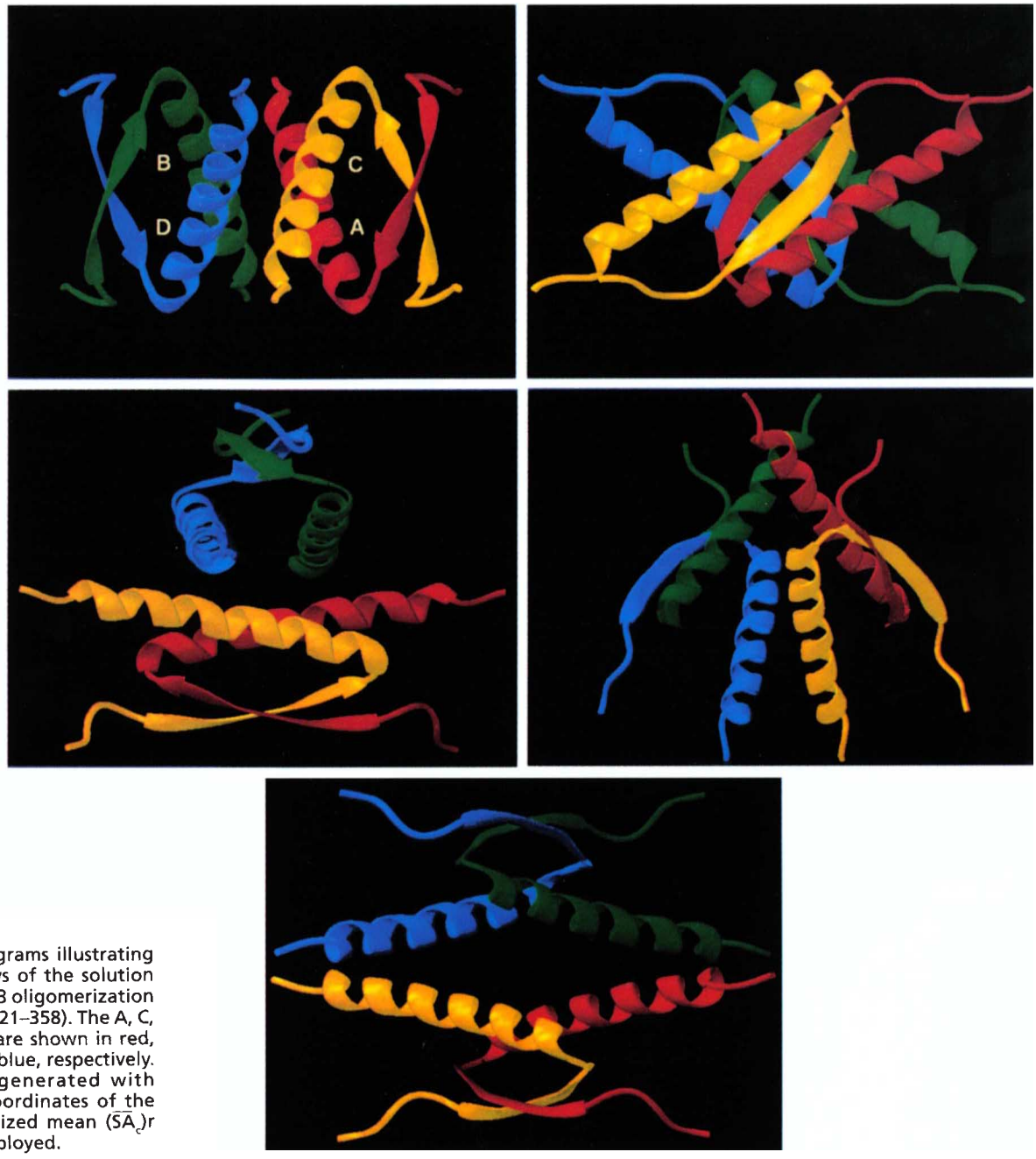

Fig. 2 Ribbon diagrams illustrating five different views of the solution structure of the p53 oligomerization domain (residues 321–358). The A, C, B and D subunits are shown in red, yellow, green and blue, respectively. The figure was generated with RIBBONS[55]. The coordinates of the restrained regularized mean $(\overline{SA}_c)r$ structure were employed.

however, that the root-mean-square difference between the mean coordinate positions of the two ensembles of structures for both the backbone and all ordered atoms is slightly larger (by 0.07–0.08 Å) than the values for the corresponding precisions (Table 3). Hence, it is clear that the uncertainties in the description of the van der Waals radii introduce uncertainties in the accuracy of the mean coordinate positions of the p53 tetramer, probably of the order of 0.1–0.2 Å for the backbone and ordered side chains[20].

Finally, it is worth noting that all the ϕ/ψ angles for all non-glycine residues within the core of the tetramer (residues 324–356) lie within the most favoured regions of the Ramachandran plot as defined by the program PROCHECK[26]. This improvement in stereochemistry is

Table 2 Structural statistics[1]

Structural statistics	<SA_c>	($\overline{SA}_c$)r	<SA_d>	($\overline{SA}_d$)r	X-ray[2]
r.m.s. deviations from experimental distance restraints (Å)[3]					
All (3752)	0.026±0.002	0.025	0.021±0.002	0.021	0.129 (30)
Intra-subunit					
intra-residue (740)[4]	0.042±0.005	0.036	0.037±0.005	0.033	0.076 (2)
sequential (852)	0.028±0.005	0.035	0.023±0.004	0.030	0.035 (0)
medium (712)	0.015±0.002	0.012	0.011±0.002	0.010	0.021 (16)
long (76)	0.005±0.006	0.000	0.002±0.004	0.005	0.000 (0)
H-bonds (136)[e]	0.002±0.003	0.000	0.002±0.003	0.000	0.365 (12)
Inter-subunit					
AC (876)	0.015±0.002	0.012	0.005±0.002	0.004	0.043 (0)
AB (244)	0.018±0.002	0.009	0.011±0.005	0.005	0.107 (0)
AD (40)	0.004±0.007	0.000	0.0005±0.001	0.000	0.000 (0)
H-bonds AC (40)[5]	0.004±0.006	0.000	0.002±0.003	0	0.000 (0)
H_2O AC (36)[5,6]	0.0002±0.0007	0.000	0.0003±0.0007	0.002	
r.m.s. deviations from experimental dihedral angle restraints (°) (284)[3,7]	0.147±0.056	0.165	0.238±0.043	0.264	1.132 (0)[b]
r.m.s. deviations from $^3J_{HN\alpha}$ coupling constants (Hz) (144)[3]	0.36±0.07	0.42	0.29±0.05	0.31	1.37
r.m.s. deviations from chemical shifts (p.p.m.)					
$^{13}C\alpha$ (152)	0.75±0.09	0.80	0.79±0.11	0.81	0.68
$^{13}C\beta$ (140)	0.92±0.04	0.93	0.93±0.02	0.96	0.92
E_{L-J} (kcal mol^{-1})[8]	−781±20	−769	−618±26	−601	−701
Deviations from idealized covalent geometry					
bonds (Å) (2,820)	0.0037±0.0002	0.004	0.002±0.0001	0.002	0.022
angles (°) (5,104)	0.520±0.028	0.605	0.442±0.018	0.479	2.08
impropers (1,444)[9]	0.292±0.068	0.416	0.253±0.071	0.276	2.42

[1]The notation of the structures is as follows: <SA_c> and <SA_d> are the ensembles of simulated annealing structures (comprising 76 individual structures each) calculated using hard sphere van der Waals' radii derived from the CHARMM[21,22,56] and ECEPP/DISMAN/DIANA[23,24] parameters, respectively (see Table 2 in ref. 20); $\overline{SA}_c$ and $\overline{SA}_d$ are the mean structures obtained by averaging the coordinates of the inidvidual structures in the <SA_c> and <SA_d> ensembles, respectively, best fitted to residues 326–354 of the four subunits combined; ($\overline{SA}_c$)r and ($\overline{SA}_d$)r are the restrained regularized mean structures obtained by restrained regularization of the mean structures SA_c and SA_d, respectively. The number of terms for the various restraints is given in parentheses and applies to the entire tetramer. The force constants for the various terms in the target function are as follows: 30 kcal mol^{-1} Å^{-2} and 200 kcal mol^{-1} rad^{-2} for the square-well interproton distance and torsion angle restraints terms, respectively; 1 kcal mol^{-1}.Hz^{-2}, 0.5 kcal.mol^{-1}.ppm^{-2}, 100 kcal mol^{-1}.Å^{-2}, 1000 kcal mol^{-1} Å^{-2}, 500 kcal mol^{-1} rad^{-2} and 500 kcal mol^{-1} rad^{-2} for the harmonic coupling constant, chemical shift, symmetry, bond, angle and improper torsion terms, respectively; and 4 kcal mol^{-1} Å^{-4} for the quartic van der Waals repulsion term.

[2]The 1.7 Å resolution crystal structure[15]. The number of interproton distance, torsion angle and $^3J_{HN\alpha}$ coupling constant violations greater than 0.5 Å, 20° and 2 Hz, respectively, are indicated in parentheses.The value quoted for the r.m.s. deviation from the torsion angle restraints excludes the two C-terminal residues of the X-ray structure, Ala 355 and Gly 356, as the deviations from the torsion angle restraints for these two residues is large (56° for Ala 355 and 120° for Gly 356) and the crystallographic *B*-factors for the backbone of Ala 355 and Gly 356 are high (50–70 Å^2), indicating that this region of the protein is poorly ordered in the crystal.

[3]None of the NMR structures exhibit distance violations greater than 0.3 Å, dihedral angle violations greater than 3°, or $^3J_{HN\alpha}$ coupling constant violations greater than 2 Hz.

[4]Only structurally useful intra-residue NOEs are included in the intra-residue interproton distance restraints. Thus, intraresidue NOEs between protons separated by two bonds or between non-stereospecifically assigned protons separated by three bonds are not incorporated in the restraints.

[5]For each hydrogen bond there are two distance restraints: r_{NH-O}, 1.7–2.5 Å and r_{N-O}, 2.3–3.5 Å.

[6]For each water molecule there are three interproton distance restraints between protein protons and water protons and five distance restraints relating to hydrogen bonds.

[7]There are 144 ϕ, 104 $\chi1$ and 36 $\chi2$ restraints (the latter include the $\chi2$ of aromatic rings restrained to 90°±30°). The minimum ranges used for the ϕ, $\chi1$ and $\chi2$ torsion angle restraints are ±10°, ±20°, and ±20°, respectively[59].

[8]E_{L-J} is the Lennard-Jones van der Waals' energy calculated with the CHARMM empirical energy function[22,57]. It is not included in the target function for simulated annealing or restrained regularization.

[9]The improper torsion restraints serve to maintain planarity and chirality.

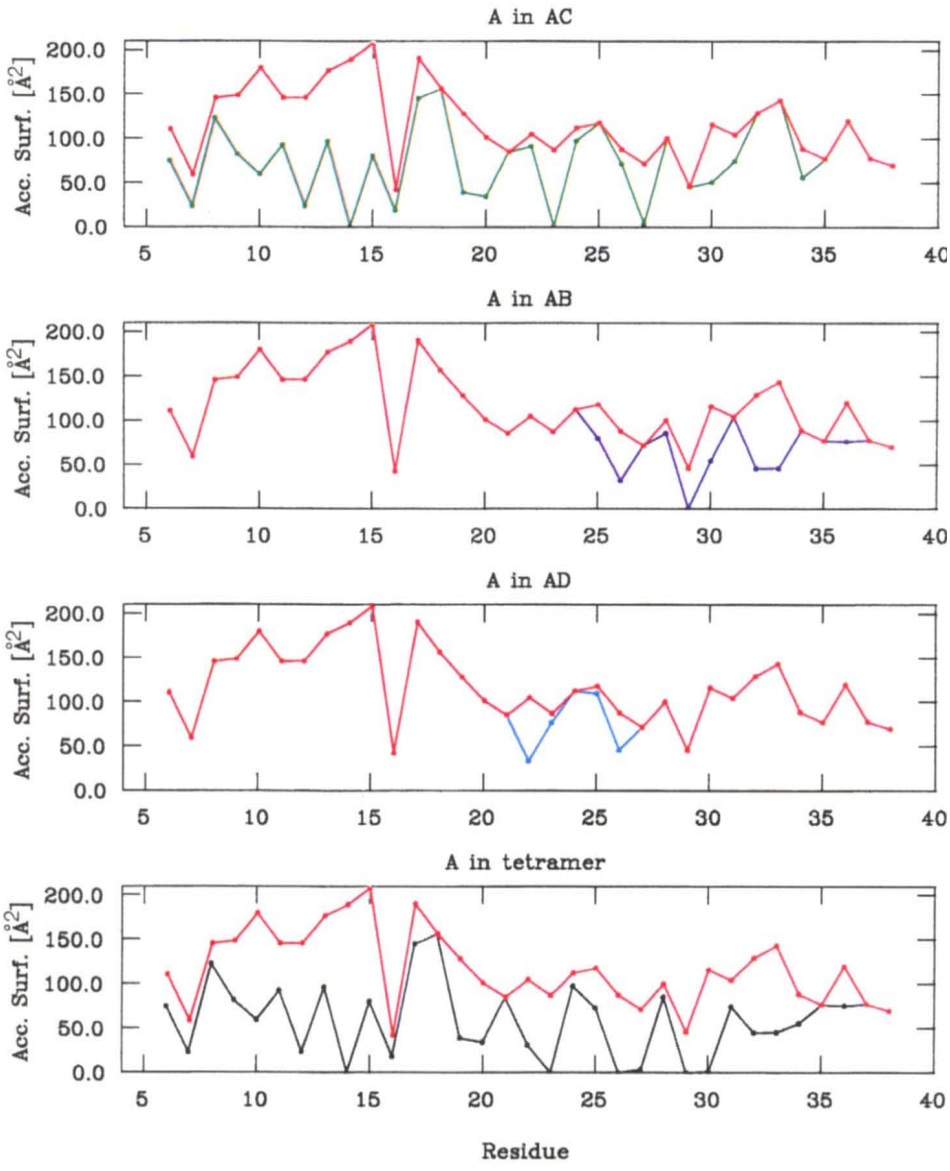

Fig. 3 Accessible surface area of the residues in subunit A on interaction with subunits C (green), B (dark blue) and D (light blue) individually; and on interaction with subunits B,C and D in the tetramer (black). For reference, the surface accessibility of subunit A in the monomer is displayed in red in each panel.

a straightforward result of the substantial increase in the number of NOE derived interproton distance restraints coupled with direct refinement against $^{3}J_{HN\alpha}$ coupling constants[19] and secondary $^{13}C\alpha$ and $^{13}C\beta$ chemical shifts[16].

Description of the structure

Views of the solution structure shown in Fig. 2*a–d* are in the same orientation as those shown in Fig. 3*a–d* of our original paper[12] to allow ease of comparison. The structure is a dimer of dimers. Each monomer is composed of a turn (Asp 324–Gly 325), a β-strand (residues Glu 326–Arg 333), a turn (Gly 334), and an α-helix (Arg 335–Gly 356), as defined by the criteria of Kabsch and Sander[27]. The N and C termini (residues 319–323 and 357–358) are completely disordered and highly mobile in solution[25].

The contacts within the primary AC dimer (composed of an antiparallel β–sheet and two antiparallel α–helices oriented at an angle of ~ 155°) are extensive. 1,397 Å² of accessible surface area per monomer (involving 22 residues per monomer) are buried on dimerizarion of subunits A and C (Fig. 3). This interaction yields a solvation free energy of dimerization[28] of –14.7 kcal mol^{-1} per monomer. The extent of the contacts between subunits A and C is illustrated by the stereoview shown in Fig. 4*a*. The β–sheet is stabilized by eight backbone hydrogen bonds. A hydrophobic core is formed by the packing of the β–sheet with the overlying α–helices and involves Phe 328, Leu 330, Ile 332, Phe 338, Phe 341 and Arg 342. Hydrophobic helix-helix contacts extend the hydrophobic core and comprise the interactions of Met 340(A) with Leu 348(C), Phe 341(A) with Leu 344(C) and Leu 348(C), Leu 344(A) with Phe 341(C) and Leu 344(C), and Leu 348(A) with Arg 337(C) and Phe 341(C). In addition there are a number of side chain hydrogen-bonding interactions between subunits A and C. In particular, there is a salt bridge between the carboxylate of Asp 352(A) and the guanidinium group of Arg 337(C), and a water-bridged hydrogen-bonding cluster involving the backbone amide of Arg 333(A), the side-chain carboxyamide of Asn 345(C) and the carboxylate of Glu 349(C). This water molecule was identified by NOE/ROEs from water to the backbone amide of Arg 333, the side-chain amide of Asn 345 and the CγmH$_3$ methyl group of Ile 332. Independent evidence for these electrostatic interactions is afforded by pH titration studies (data not shown). In particular, the chemical shifts of the side-chain Cγ atom of Asp 352 and the NεH of Arg 337 show complex titration behaviour with one pK_a < 3; and the chemical shifts of the backbone amide group of Arg 333, the side-chain amino group of Asn 345 and the Cδ atom of Glu 349 titrate with a pK_a ~ 3.6. The pK_a of the carboxylate of Asp 352 is substantially lower than that for a free Asp (pK_a ~ 3.7–3.9) indicating a strong salt bridge interaction with its positively charged partner Arg 337.

While the accessible surface area buried per monomer (572 Å²) on tetramerization is a factor of about 2.5 times less than that buried upon dimerization (1,397 Å²), the total accessible surface area buried on

tetramerization (2,290 Å^2), that is on the association of the two primary dimers, is only slightly less than that buried on dimer formation (2,793 Å^2). A total of ten residues per monomer, are buried on tetramerization, six due to AB contacts alone, two due to AD contacts alone and two due to both AB and AD contacts (Fig. 3). The solvation free energy of tetramerization per monomer is –5.3 kcal mol^{-1} which can be partitioned into ~ 3.35 kcal mol^{-1} arising from the interaction of subunits A and B, and –1.95 kcal mol^{-1} arising from the interaction of subunits A and D. The total solvation free energy of tetramerization is –21.2 kcal mol^{-1} compared to a value of –29.3 kcal mol^{-1} for the total solvation free energy of dimerization. The total solvation free energy of folding for the tetramer is ~ –140 kcal mol^{-1} which is what one would expect for a protein of this size[29].

The A and B helices are oriented in an approximately orthogonal manner at an angle of ~ 81°. Hydrophobic contacts occur between Leu 344(A), Leu 344(B) and Leu 348(B); between Ala 347(A), Ala 347(B), Leu 348(B) and the hydrophobic portion of Lys 351(B); and between Leu 350(A), Leu 350(B) and the hydrophobic portion of Lys 351(B) (Fig. 4*b*). There is one inter-subunit hydrogen bond between the NζH$_3^+$ of Lys 351(A) and the backbone carbonyl of Glu 343(B) which can be identified unambiguously from the structures (Fig. 4*b*). Helices A and D are also oriented approximately orthogonally but with an interhelical angle of ~ –104°. The hydrophobic contacts between subunits A and D are entirely hydrophobic and involve Met 340, Phe 341, Leu 344 and the hydrophobic portion of the side chain of Glu 343 (Fig. 4*c*).

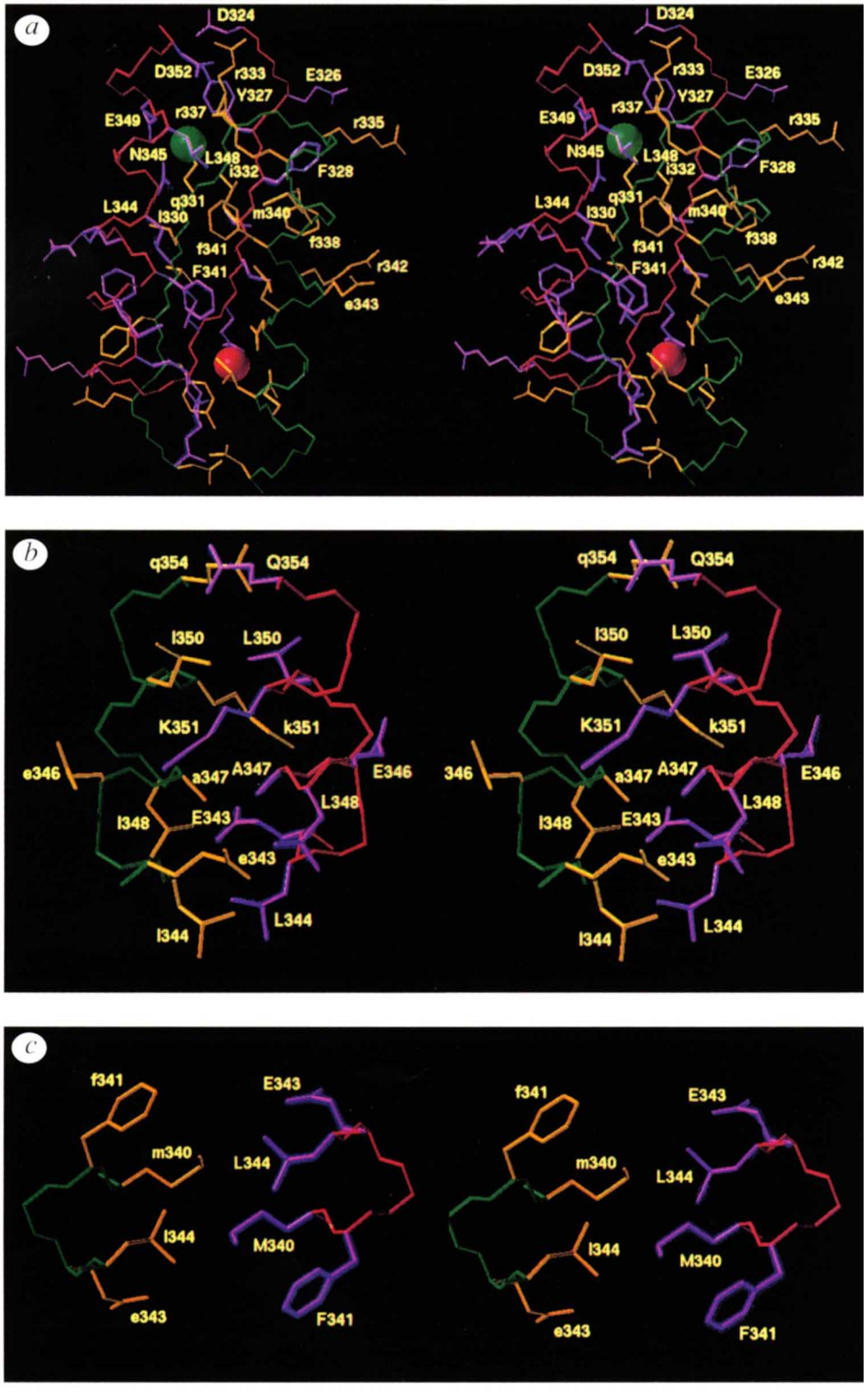

Fig. 4 Stereoviews of the *a*, AC; *b*, AB and *c*, AD interfaces for the restrained regularized mean $(\overline{SA_r})r$ structure. The backbone (N, Cα, C atoms) and side chains of subunit A are shown in red and purple, respectively, with the residues labelled with capital letters; the backbone and side chains of the other subunit are shown in green and yellow, respectively, with the residues labelled with small letters. In (*a*), the two symmetrically related water molecules within the primary dimer are shown as solid spheres. The figure was generated with VISP[56].

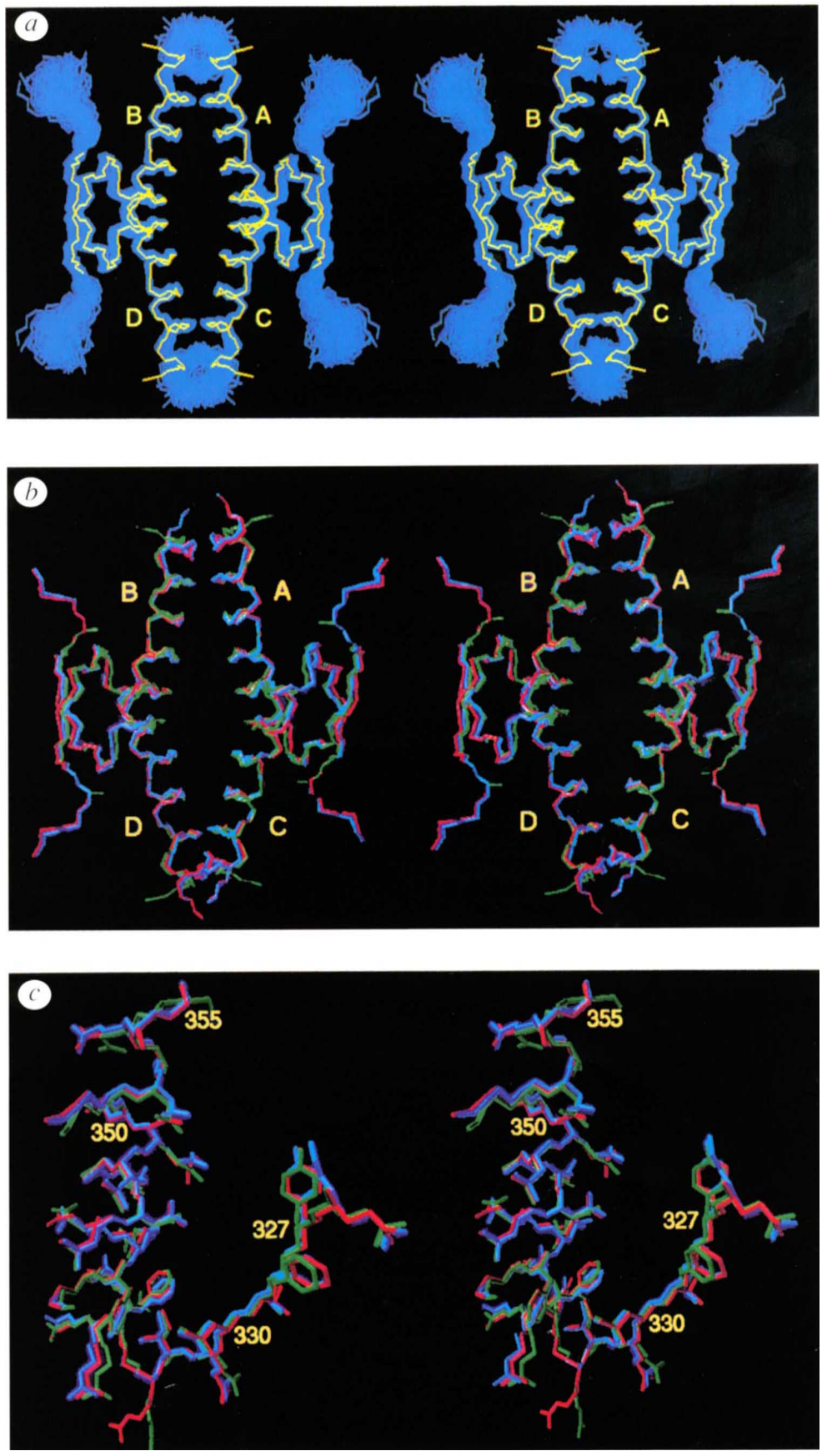

Fig. 5 Comparison of the solution and X-ray structures. *a*, Best fit superposition of the backbone (N, Cα, C) atoms of the <SA_c> and <SA_d> ensemble of structures in blue and the X-ray structure in yellow for the complete tetramer. *b*, Best fit superposition of the restrained regularized mean ($\overline{SA}_c$)r (red) and ($\overline{SA}_d$)r (blue) structures and the X-ray structure (green) for the complete tetramer. *c*, Best fit superposition of the backbone and side chains (residues 327–355) of the restrained regularized mean ($\overline{SA}_c$)r (red) and ($\overline{SA}_d$)r (blue) structures and the X-ray structure (green) for the monomer. Note that a total of 152 simulated annealing structures are superimposed in (*a*), and that in (*a*) and (*b*) residues 322–357 are displayed for the simulated annealing structures and residues 325–356 for the X-ray structure. (Note that only residues 325–356 are visible in the electron density map[15].) (*a*) was generated with AVSXPLOR[54], and (*b*) and (*c*) VISP[56].

Table 3 Atomic r.m.s. differences[1]

	Atomic r.m.s. difference (Å)		
	Backbone[2] atoms	All atoms	All ordered[3] atoms
NMR structures (tetramer)			
$\langle SA_c \rangle$ against $\overline{SA}_c$	0.32±0.06	0.77±0.09	0.37±0.06
$\langle SA_d \rangle$ against $\overline{SA}_d$	0.32±0.06	0.73±0.07	0.37±0.05
SA_c against $\overline{SA}_d$	0.39	0.50	0.44
NMR against X-ray structures[4]			
Tetramer			
$\langle SA_c \rangle$ against X-ray	0.68±0.09	1.23±0.04	0.76±0.07
$\langle SA_d \rangle$ against X-ray	0.73±0.09	1.30±0.09	0.80±0.08
$(\overline{SA}_c)r$ against X-ray	0.59	0.98	0.66
$(\overline{SA}_d)r$ against X-ray	0.65	1.15	0.72
AC dimer			
$\langle SA_c \rangle$ against X-ray	0.58±0.08	1.19±0.08	0.65±0.06
$\langle SA_d \rangle$ against X-ray	0.70±0.09	1.28±0.09	0.77±0.07
$(\overline{SA}_c)r$ against X-ray	0.50	0.97	0.55
$(\overline{SA}_d)r$ against X-ray	0.65	1.14	0.70
Monomer			
$\langle SA_c \rangle$ against X-ray	0.44±0.05	1.14±0.08	0.56±0.04
$\langle SA_d \rangle$ against X-ray	0.56±0.05	1.23±0.09	0.68±0.05
$(\overline{SA}_c)r$ against X-ray	0.38	0.93	0.48
$(\overline{SA}_d)r$ against X-ray	0.52	1.10	0.63

[1]The notation of the structures is defined in footnote 1 to Table 2. The r.m.s. difference between the mean coordinates, $\overline{SA}_c$ or $\overline{SA}_d$, and their respective restrained regularized mean coordinates, $(\overline{SA}_c)r$ or $(\overline{SA}_d)r$, is ~0.1 Å for backbone atoms, 0.34–0.38 Å for all atoms and 0.11–0.13 Å for all ordered atoms.
[2]The backbone atoms comprise the N, Cα, C, and O atoms of residues 326–354.
[3]The atoms that do not exhibit conformational disorder comprise all N, Cα, C, O and Cβ atoms of residues 326–354 of the four subunits; the complete side chains of Y327, F328, T329, L330, I332, F338, M340, F341, L344, L348 and L350; the side chains of D324, E326, E331, R333, R335, R337, E339, E343, E346, E341 and D352 up to Cγ, of R342 up to Cδ, and K351 up to Cε; and the four water molecules (one per subunit)
[4] In the comparisons with the X-ray structure, we quote the values for the r.m.s. differences between the restrained regularized mean NMR coordinates and the X-ray structure rather than those between the mean NMR coordinates and the X-ray structure. The differences between these values is <0.01 Å for backbone atoms and all ordered atoms, and ≤0.05 Å for all atoms.

Comparison with the crystal structure

The solution and X-ray structures are very similar at the monomer, dimer and tetramer levels (Fig. 5, Table 3). The overall backbone atomic r.m.s. differences between the mean coordinates of the $\langle SA_c \rangle$ and $\langle SA_d \rangle$ ensembles and the X-ray structures are 0.60 Å and 0.65 Å, respectively, (compared to values of 1.9 Å and 1.2 Å for the NMR structures of Lee *et al.*[14] and Clore *et al.*[13]). Taking into account the uncertainties of 0.1–0.2 Å arising from the description of the non-bonded contacts (compare the differences between the $\langle SA_c \rangle$ and $\langle SA_d \rangle$ ensembles presented in Table 4), we can estimate the likely accuracy of the mean coordinates from the precision of the ensembles of simulated annealing sructures, assuming that there are no systematic errors in the experimental restraints[20]. The estimated accuracy ranges from about 0.5–0.6 Å for the backbone atoms to 0.6–0.7 Å for the ordered side chains. Given, the coordinate uncertainties of 0.2–0.3 Å expected for a 1.7 Å resolution crystal structure refined to an *R*-factor of 19.2 %[15], the structures in solution and in the crystal are very similar indeed. In contrast to the earlier NMR structures[13], the present ensembles of solution structures show no evidence of expansion relative to the X-ray structure. This is entirely due to the substantial increase (approximately 3.5 fold) in the number of NOE restraints between the two dimers.

The r.m.s. differences between the $\langle SA_c \rangle$ ensemble of structures and the X-ray structure is systematically smaller than that between the $\langle SA_d \rangle$ ensemble of structures and the X-ray structure at the tetramer, dimer and monomer levels. Moreover, whereas at the tetramer level, this difference (for both backbone and ordered side chains) is only ~ 0.05 Å, at the monomer and dimer levels it is around ~ 0.15 Å. At the tetramer level, the uncertainties in the orientation of the two dimers is primarily due to the limited number and precision of the interdimer NOEs (a total of 284). The number of intersubunit NOEs (476, including hydrogen-bonding restraints) in each dimer, however, is substantially larger than that between the two dimers. Under these conditions, the contribution to the coordinate uncertainties engendered by the description of the non-bonded contacts increases in prominence. Likewise at the monomer level, the conformation of the monomer is not only determined by a large number of intra-monomer NOEs (namely, 629 including hydrogen-bonding restraints) in conjuction with coupling constant, $^{13}C\alpha$ and $^{13}C\beta$ secondary chemical shift and torsion angle restraints, but also by all the inter-subunit NOEs. Here too the limitations imposed by the non-bonded contacts increase in relative importance.

On the basis of an evaluation of the measured coupling constants there appear to be minor differences between the solution and published X-ray structures. The r.m.s. deviation between observed and calculated $^3J_{HN\alpha}$ coupling constants for the X-ray structure[15] is 1.6 Hz, with ten residues (326, 328, 329, 331, 332, 338, 341, 348, 352 and 354) having coupling constants that differ by more than 1.5 Hz, of which five (residues 328, 329, 331, 341 and 354) differ by more than 2 Hz. For highly refined X-ray structures, the agreement is between 0.5 and 0.8 Hz[30]. The $^3J_{CC}$ coupling constants involving the methyl groups of Thr 329 and Leu 350 have values of ~ 2 Hz indicative of rotamer averaging about $\chi 1$ and $\chi 2$, respectively, in solution[31]. In the crystal structure, on the other hand, the side chains of both these residues appear to be in only a single conformation with a $\chi 1$ of 60° and a $\chi 2$ of 180°, respectively, and are characterized by low *B*-factors[15]. Finally, in the crystal structure there is a hydrogen bond between the hydroxyl group

of Tyr 327(A) and the guanidinium group of Arg 333(B)[15]. In solution, we see no NOEs that would indicate that these two groups are sufficiently close in solution to form a hydrogen bond; for example, no NOE was observed between the CεH ring protons of Tyr 327 and the NεH of Arg 333, although in the crystal structure this distance is ~3.5 Å.

Relationship to biochemical data

Stürzbecher *et al.*[32] examined the oligomerization properties of a multiple mutant in which Phe 341, Leu 344, Leu 348 and Ala 355 were substituted by Lys, Glu, Glu and Lys, respectively, and found it to be entirely monomeric. These mutations affect both the dimerization and tetramerization interfaces. In particular, the Phe 341 → Lys mutation will destabilize the hydrophobic core within the AC dimer formed by the interaction of the β–sheet with the overlying helices; the Leu 344 → Glu will destabilize hydrophobic inter-helical contacts at the AC, AB and AD interfaces and, finally the Leu 348 → Glu mutation will destabilize interhelical contacts at the AC and AB interfaces (Figs 3, 4).

Sakamoto *et al.*[33] examined the oligomerization properties of a series of synthetic peptides derived from the oligomerization domain. They found that peptides comprising residues 332–360 and 335–393 were entirely monomeric. In both these peptides, the residues that form the β–sheet in the AC dimer are removed (Fig. 4*a*). Given that all the residues at the tetramer interface are preserved in these peptides, these results imply that the formation of the primary dimer is an essential prerequisite for tetramer formation, and that the presence of the β–sheet is an absolute requirement for dimer formation. This is further supported by the results on a peptide from residues 319–360 in which Leu 323, Tyr 327 and Leu 330 are substituted for Ala. This peptide is also completely monomeric in solution. While the Leu 323 → Ala substitution should have no effect upon oligomerization, the Tyr 327 → Ala substitution will reduce the strength of the hydrophobic interaction between the aromatic ring of Tyr 327(A) and the aliphatic portion of the side chain of Arg 333(C), and the Leu 330 → Ala substitution is likely to introduce a destabilizing cavity within the core of the dimer (Fig. 4*a*).

The most extensive biochemical data has recently been obtained by Waterman *et al.*[34] who examined the effects of a whole series of single and multiple mutations within the oligomerization domain on the DNA-binding properties of intact p53. The following single mutations had no effect on DNA-binding of intact p53: Tyr 327 → Ile; Phe 328 → Ala; Phe 338 → Ala; Phe 341 → Leu; Leu 350 → Ala; Lys 351 → Ala or Leu; Gln 354 → Arg; Ala 355 → Leu; and Gly 356 → Ala. Many of these results are entirely expected on the basis of the structure. Tyr 327(A) is located on the solvent exposed surface of the β–sheet, and is in contact with the aliphatic portion of the side chain of Arg 333(C) (Fig. 4*a*). Substitution of Tyr 327 with a long aliphatic side chain, such as Ile, should not affect this hydrophobic interaction. Phe 328(A) is located at the outer edge of the AC hydrophobic core and is packed against the aliphatic portion of the side chain of Arg 335(C) and Phe 338(C) (Fig. 4*a*); substitution for an Ala should still permit some hydrophobic contacts to occur. Similarly Phe 338(A) is located at the outer edge of the AC hydrophobic core (Fig. 4*a*) so that an Ala substitution should still permit hydrophobic contacts with Phe 328(C) and the aliphatic portion of the side chain of Arg 342(A). Phe 341 is located within the core of the AC dimer but there is no reason not to expect that a conservative substitution with a Leu should not be completely tolerated, particularly as a Leu residue is conformationally flexible[35,36]. Interestingly, the Phe 341 → Ile mutant displayed slightly decreased DNA binding. The conformational entropy of the branched side chain of Ile is less than that of the Leu side chain[34]. This leads one to predict that it is more difficult to accommodate Ile than Leu within the hydrophobic core and, as a result, the Phe 341 → Ile substitution may slightly destabilize the AC dimer. Ala 355 and Gly 356 are located at the C termini of the α-helix and do not partici-

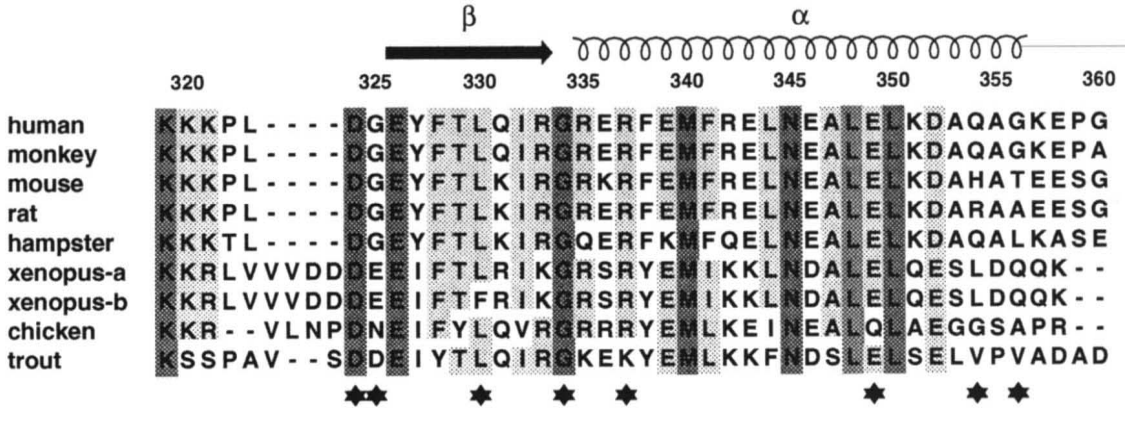

Fig. 6 Sequence alignment of the oligomerization domain of p53 from various organisms ranging from trout to man. Residues that are absolutely conserved are heavily shaded, and residues that display ≥75 % similarity are lightly shaded. The sites of the eight point mutations identified in human cancers[37] are indicated by asterisks, and the secondary structure of the oligomerization domain is shown above the sequences.

pate in any intersubunit interactions so that substitutions at these positions should have no effect on the integrity of the tetramer.

Leu 350 and Lys 351 play an important role in the AB interface that constitutes the main site of interaction of the two dimers (AC and BD) to form the tetramer (Figs. 3, 4*b*). While the Lys 351 → Leu mutation might have little effect on the stability of the AB interaction as a long hydrophobic side chain that can still make extensive hydrophobic contacts is preserved, one would expect both the Leu 350 → Ala and Lys 351 → Ala mutations to significantly shift the dimer-tetramer equilibrium towards the dimer. The observation that the mutations at these positions appear to be silent with regard to DNA-binding of intact p53[34] therefore suggests one of two possibilities: either, the strength of the dimer-dimer interaction is significantly reduced but tetramerization can still occur efficiently on the DNA, or these mutations are accomodated at minimal expense. In the case of the Leu 350 → Ala mutant, the methyl group of Ala could still interact with the CαH of Lys 351, while in the case of the Lys 351 → Ala mutant, the methyl group of Ala could still interact with Leu 350. Only structural data on these mutants will shed light on these different possibilities. What is clear, however, is that the results on the substitutions of Lys 351 by aliphatic side chains indicate that the hydrogen bond between the $N\zeta H_3^+$ of Lys 351(A) and the backbone carbonyl of Glu 343(B) is not an essential determinant of tetramerization.

The data on the Gln 354 → Arg mutant are of interest as this mutation has been found in human cancers[37], although apparently it has no effect on DNA binding *in vitro*[34]. Gln 354 is the C terminal most residue involved in the interaction surface of the A and B subunits (Fig. 4*b*). There exists the possibility of water bridged hydrogen-bonding between the carboxyamide group of Gln 354(A) and either the carboxyamide group of Gln 354(B) and/or the backbone carbonyl of Leu 350(B) which are separated by 5.5–6.0 Å. We have no direct evidence for the presence of a water molecule at this location, however, as an exchange cross-peak, rather than a ROE cross peak, is observed between the side-chain amide of Gln 354 and water in the 2D H_2O-selective ROE-^1H-^{15}N HSQC spectrum. An Arg could substitute for Gln at this position, which would be in agreement with the observation that it does not perturb DNA binding *in vitro*. The double [Phe 341,Leu 344] → [Leu,Ile] mutant also had no effect on DNA binding[34]. Leu 344 participates in the AC, AB and AD interfaces (Figs 3,4), however, both substitutions are conservative and would therefore be expected to have little effect.

Two mutations involving the connection between the β-strand and the helix (Fig. 4*a*) were found to compromise but not abolish DNA binding of intact p53, namely Gly 334 → Gln and [Arg 335,Glu 336] → [Gly,Gly][34]. Gly 334 has an unusual backbone conformation with φ/ψ angles of 86°/140° which are usually only accessible to Gly. This conformation, however, is close to that of the N-cap residue in N-terminal helix capping boxes which generally cluster around $\phi = 94 \pm 15°$ and $\psi = 167 \pm 5°$ (ref. 38). While a positive φ angle for a Gln is generally unfavourable, the deleterious effects of steric clash could be compensated, at least partially, by a side chain to backbone hydrogen bond between the carboxyamide side chain of the Gln at position 334 and the backbone amide of Arg 337. Arg 335 and Glu 336 constitute the first two residues of the helix. Their substitution by Gly will certainly perturb the starting point of the helix and may consequently reduce the stability of the AC dimer sufficiently to reduce the DNA-binding affinity of intact p53.

The triple mutant [Gly 334, Arg 335,Glu 336] → [Ala,Gln,Ala], on the other hand, has no DNA binding activity at all[34]. We suspect that this can be entirely attributable to the substitution of Gly 334 by Ala, as the side chains of the other two residues are located on the solvent exposed surface of the protein and do not participate in any interactions with other side chains. Unlike Gln, Ala cannot participate in any side chain to backbone-hydrogen bonding interactions, and the presence of the bulky methyl group is likely to introduce a sufficient steric clash to severely distort the turn between the strand and the helix and hence the angle between them. While a negative φ angle for an Ala at position 334 could potentially be accomodated by the structure, this would alter both the intra-monomer angle between the β-strand and the helix, as well as the intersubunit AC interhelical angle within the dimer, thereby potentially reducing the strength of the AC interaction. The importance of maintaining the angles between these structural elements is further supported by the observation that the introduction of a Gly between Gly 334 and Arg 335 results in a molecule that no longer binds DNA.

The three mutants Arg 337 → Leu and [Gly 334,Arg 337] → [Leu,Ile] or [Phe,Leu] completely abolished DNA binding[34]. Mutation of Arg 337 to any hydrophobic residue will remove the salt bridge between the side chains of Arg 337(A) and Asp 352(C) (Fig. 4*a*). In the case of the double mutant, this effect will be further compounded by severe steric clash following the replacement of Gly 334 by an entirely hydrophobic side chain for the reasons discussed in the previous paragraph.

Finally, one mutant, Leu 344 → Ala, was found to bind to DNA in a dimeric state[34]. Leu 344 is mainly involved in hydrophobic contacts at the tetramerization interface of the two primary dimers (Figs 3, 4*b*, *c*). Introduction of the much smaller Ala residue at this position would introduce a destabilizing cavity at this interface, thereby dissociating the tetramer into the primary dimers.

Mutations found in tumours

The vast majority of p53 mutations found in human cancers are located in the DNA-binding domain of p53[1–5,37]. Nevertheless, a number of mutations are found within the oligomerization domain[37]. The importance of the oligomerization domain for p53 function both *in vitro* and *in vivo* is documented by a number of findings: stop mutations just prior to the oligomerization domain at residues 317 and 319 have been found in human cancers[38]; the oligomerization domain is responsible for the negative dominant mechanism whereby heterotetramers of wild type and mutant (DNA domain) p53 either no longer bind DNA or bind with much reduced affinity[39,40]; the oligomerization properties of a minimal transforming unit (residues 302–360) are responsible for abrogat-

ing p53 activity by forming hetero-oligomers with wild type p53, thereby reducing the concentration of wild type homotetrameric p53 (ref. 41); oligomerization is required for DNA binding of *in vitro* translated p53 (42,43); and it has been demonstrated that mutations within the oligomerization domain can abolish DNA binding of intact p53 *in vitro*[35]. It is therefore of interest to rationalize the mutations within the oligomerization domain that have been identified in tumours on the basis of the structure of the oligomerization domain.

Three stop mutations at the positions of Gln 331, Glu 339 and Arg 342[37,44] are of interest. Gln 331 is located in the middle of the β-strand so that chain termination at this point would completely obliterate oligomerization. Chain termination at Glu 339 and Arg 342 would remove all contacts between subunits A and B, and either all or half the contacts, respectively, between subunits A and D, thereby severely destabilizing the assocation of the two dimers to form a tetramer (Figs 3, 4*b*,*c*). In addition, these two stop mutations would remove the two inter-subunit side chain hydrogen-bonding interactions within the dimer discussed above.

To date eight point mutations within the oligomerization domain have been identified in human cancers[37], and the effects of four, Leu 330 → His, Gly 334 → Val, Arg 337 → Cys and Glu 349 → Asp, can be clearly explained in terms of the structure and the destabilization of the primary dimer. The consequences of the remaining four mutations, Asp 324 → Glu, Gly 334 → Val, Gln 354 → Arg (which was discussed in the previous section) and Gly 356 → Trp, are not immediately apparent from the structure.

The Leu 330 → His mutation substitutes a completely buried hydrophobic residue by a polar residue in the centre of the hydrophobic core of the primary dimer (Figs. 3, 4*a*). The effects of the Gly 334 → Val mutation will be similar to those of the Gly 325 → Ala mutation[34] discussed in the preceeding section. Like Ala, a Val residue cannot accomodate a positive φ angle in the absence of severe steric clash, and any change in φ angle at this position, together with any compensatory changes in the backbone torsion angles of the adjacent residue, will distort the angle between the strand and the helix and the consequent packing of the helices in the AC dimer. The Arg 337 → Cys mutation, like the Arg 337 → Leu mutation[34], removes a salt bridge between the guanidinium group of Arg 337(A) and the carboxylate of Asp 352(C) (Fig. 4*a*). Finally, the Glu 349 → Asp mutation would probably remove a water-bridged hydrogen-bonding interaction between the carboxylate of Glu 349(A) and the backbone amide of Arg 333(C) (Fig. 4*a*), as the Asp side chain is likely to be too short to permit this hydrogen bond to occur.

Asp 324 and Gly 325 are located in the turn preceeding the β-strand (Fig. 4*a*). In the present ensemble of structures, there is a potential intra-monomer hydrogen bond between the carboxylate side chain of Asp 324 and the hydroxyl group of Tyr 329 which may stabilize this turn. The backbone coordinates of this turn, however, are only defined to a precision of 1 Å, and the side chain of Asp 325 is only defined to a precision of about 2 Å. Even though this region is highly mobile[25], the Asp 324 → Glu and Gly 325 → Val mutations may distort the conformation of the turn, thereby potentially altering the relative orientation of the DNA-binding and oligomerization domains sufficiently to reduce the DNA-binding affinity. It should be noted, however, that the linker between the oligomerization and DNA-binding domains is 30 residues in length so that one might predict that a change in the conformation of the turn at positions 324–325 could easily be accomodated.

Gly 356 is the C-terminal residue of the α-helix but is not involved in any inter-subunit interactions. As the Cα-Cα separation between Gly 356 of subunits A and B is 22.5 Å, one would not expect the Gly 356 → Trp mutation to affect oligomerization, particularly as the Gly 356 → Ala mutation[34] discussed in the previous section has no effect on DNA binding. On the other hand, Trp is a very bulky residue and may well interfere with C-terminal helix-capping[45].

Evolutionary considerations

p53 sequences have only been detected in vertebrates[46] and a sequence alignment of the oligomerization domain from several organisms, spanning approximately 400 million years of evolutionary history (from the point of the origin of the bony fishes) is shown in Fig. 6. The sequences show obvious regions of conservation that can be correlated with the structure of the tetramer and provide a series of natural variants with which to examine the consequences of amino acid substitutions. Sequence identity for residues 319–360 varies from 97.6 % (human against green monkey) to 40.5 % (human against trout). There are approximately 110 PAM units (accepted point mutations) between humans and trout, yielding a mutation rate somewhere between that of haemoglobins and heavy chain constant regions[47]. Within the mammals, the oligomerization domain shows greater sequence conservation than for the whole protein (data not shown).

The p53 oligomerization domain (residues 319–360) has 8 out of 42 positions that are absolutely conserved and 24 out of 42 positions that are highly conserved (>75% similarity). Differences primarily cluster in the N- and C-terminal regions which are disordered in solution. This includes variable length insertions in the N-terminal region and radical sequence divergence in the C-terminal region. Of the eight point mutations that have been identified in human tumours[37], five occur in highly conserved regions, providing additional evidence for their importance in maintaining the structural integrity of the tetramer. The residues at the remaining three mutation sites (Gly 325, Gln 354 and Gly 356) are highly variable, suggesting that these mutations may not in fact be deleterious to the function of p53 but simply represent incidental findings. This would be in agreement with the conclusions derived on the basis of the structure of the oligomerization domain.

In this paper, we have presented a refined solution structure of the oligomerization domain of p53, based on a substantial increase in the number of inter-subunit NOEs, particularly at the tetramerization interface, over previous NMR structure determinations[12–14]. The present solution structure is very similar to the X-ray structure[15], resolving any controversies relating to possible differ-

ences between the solution and crystal states. The current wild-type solution structure of the oligomerization domain of p53 provides a wealth of structural information that will serve as a guide for further biochemical investigations aimed at probing structure-function relationships, understanding the consequences of clinical mutations, protein engineering and possible structure-based drug design.

Methods

The expression and purification of the isotopically labelled (^{15}N or ^{15}N/^{13}C) oligomerization domain (residues 319–360) of p53 was as described previously[12]. All NMR experiments were carried out at 35 °C on a BrukerAMX600 spectrometer equipped with a z-shielded gradient triple resonance probe. The analysis of the data was based on the ^{1}H, ^{15}N and ^{13}C assignments obtained previously[12] (PDB accession code 1OLH_MR). Approximate interproton distance restraints, classified into four ranges, 1.8–2.7 Å (1.8–2.9 Å for NOEs involving NH protons), 1.8–3.3 Å (1.8–3.5 Å for NOEs involving NH protons), 1.8–5.0 Å and 1.8–6.0 Å, corresponding to strong, medium, weak and very weak NOEs, were derived from an analysis of the following multidimensional heteronuclear-filtered and -separated NOE spectra recorded in ref. 12: namely, 3D ^{15}N-separated, 3D ^{1}H-^{15}N HMQC-NOE-HSQC, 3D ^{13}C-separated, 3D ^{13}C-separated(F_2)/^{12}C-filtered(F_3), 3D ^{15}N-separated(F_2)/^{12}C-filtered (F_3) NOE, 4D ^{15}N/^{13}C-separated and 4D ^{13}C/^{13}C-separated NOE spectra recorded with mixing times of 110–120 ms. Examples of the quality of the NOE data were provided in refs. 12 and 13. Stereospecific assignments of methylene protons and methyl groups of Val and Leu, torsion angle restraints and $^{3}J_{HN\alpha}$ coupling constants were unchanged from our previous structure determination[12,13]. Bound water was identified by recording 2D water selective ^{12}C-filtered H_2O-ROE-^{1}H-^{13}C, H_2O-NOE-^{1}H-^{13}C and H_2O-ROE-^{1}H-^{15}N HSQC spectra[17,18], with mixing times of 25 and 50 ms for the ROE spectra and 50 and 100 ms for the NOE spectra. The pH dependence of the chemical shifts of backbone amide groups, the side-chain NεH group of Arg and the side-chain amino group of Asn and Gln was examined by recording a series of 19 ^{1}H-^{15}N HSQC spectra[48] over the pH range 2.13–8.75. The pH dependence of the chemical shifts of the Cγ atom of Asp and Asn and of the Cδ atom of Glu and Gln was examined by a series of six modified constant time HCACO spectra[49] over the pH range 3.1–7.18.

The structures were calculated with the hybrid distance geometry-simulated annealing protocol[21] essentially as described in ref. 12, using X-PLOR-31 (ref. 49) which had been modified to permit direct refinement against $^{3}J_{HN\alpha}$ coupling constants[19] and secondary ^{13}Cα and ^{13}Cβ chemical shifts[16]. The minimized target function therefore comprised effective harmonic potential terms for covalent geometry (bonds, angles and improper torsions), symmetry, coupling constant restraints and ^{13}C chemical shift restraints; effective quadratic square-well potential terms for the inter-proton distance and torsion angle restraints; and an effective quartic van der Waals repulsion term for the non-bonded contacts. No hydrogen-bonding, electrostatic or 6–12 Lennard-Jones empirical energy terms were present in the target function. Distances involving methyl groups, aromatic ring protons and non-stereospecifically assigned methylene protons were represented as a $(\Sigma r^{-6})^{-1/6}$ sum[51], thereby obviating the need to add corrections to the upper limits for these restraints. The symmetry restraints ensured that the atomic r.m.s. difference between the subunits in each simulated annealing structure was ≤ 0.001 Å (ref. 52). Refinement was carried out in an iterative manner[53], thereby permitting all structurally useful intra- and inter-subunit NOEs to be assigned explicitely.

The coordinates of the $\langle SA_c \rangle$ and $\langle SA_d \rangle$ ensembles of simulated annealing structures (76 structures in each ensemble), the coordinates of their corresponding restrained regularized mean structures, $(\overline{SA}_c)r$ and $(\overline{SA}_d)r$, and a complete listing of the experimental NMR restraints have been deposited in the Brookhaven Protein Data Bank.

Received 24 January; accepted 21 February 1995.

Acknowledgements
We thank N. Pavletich for providing us with the coordinates of the crystal structure of the oligomerization domain prior to publication and for useful discussion; T. Halazonetis for providing us with a preprint of his mutational data prior to publication; D. Garrett and F. Delaglio for software support; R. Tschudin for hardware support; and A. Bax and A. Szabo for stimulating discussions. R.T.C. acknowledges a Leukemia Society of America post-doctoral fellowship. This work was supported by the AIDS Targeted Antiviral Program of the Office of the Director of the National Institutes of Health (G.M.C., A.M.G. and E.A.).

1. Nigro, J.M. *et al.* Mutations in the p53 gene occur in diverse human tumour types. *Nature* **342**, 705–708 (1989).
2. Takahashi, T. *et al.* p53: A frequent target for genetic abnormalities in lung cancer. *Science* **246**, 491–494 (1989).
3. Hollstein, M., Sidransky, B., Vogelstein, B. & Harris, C.C. p53 mutations in human cancers. *Science* **253**, 49–53 (1991).
4. Lane, D.P. p53, guardian of the genome. *Nature* **358**, 15–16 (1992).
5. Harris, C.C. p53: At the crossroads of molecular carcinogenesis and risk assessment. *Science* **262**, 1980–1981 (1993).
6. Unger, T., Sau, M.M., Segal, S. & Minna, J.D. p53: A transdominant regulator of transcription whose function is ablated by mutations occuring in human cancer. *EMBO J.* **11**, 1383–1390 (1992).
7. Prives, C. & Manfredi, J.J. The p53 tumour suppresor protein: Meeting review. *Genes Develop.* **7**, 529–534 (1993).
8. Pavletich, N.P., Chambers, K.A. & Pabo, C.A. The DNA-binding domain of p53 contains four conserved regions and the major mutation hot spots. *Genes Develop.* **7**, 2556–2564 (1993).
9. Bargonetti, J., Manfredi, J.J., Chen, X., Marshak, D.R. & Prives, C. A proteolytic fragment from the central region of p53 has a marked sequence-specific DNA-binding activity when generated from wild-type but not oncogenic mutant p53 protein. *Genes Develop.* **7**, 2565–2574 (1993).
10. Wang, Y. *et al.* p53 domains: Identification and characterization of two autonomous DNA binding regions. *Genes Develop.* **7**, 2575–2586 (1993).
11. Cho, Y., Gorina, S., Jeffrey, P.D. & Pavletich, N.P. Crystal structure of a p53 tumour-suppressor-DNA complex: understanding tumorigenic mutations. *Science* **265**, 346–355 (1994).
12. Clore, G.M. *et al.* High-resolution structure of the oligomerization domain of p53 by multidimensional NMR. *Science* **265**, 386–391 (1994).
13. Clore, G.M. *et al.* Interhelical angles in the solution structure of the oligomerization domain of the tumour suppressor p53. *Science* (1995).
14. Lee, W. *et al.* Solution structure of the tetrameric minimum transforming domain of p53. *Nature struct. Biol.* **1**, 877–890 (1994).
15. Jeffrey, P.D., Gorina, S. & Pavletich, N.P. Crystal structure of the tetramerization domain of the p53 tumor suppressor at 1.7 Å. *Science* (1995).
16. Kuszewski, J., Qin, J, Gronenborn, A.M. & Clore, G.M. The impact of direct refinement against $^{13}C\alpha$ and $^{13}C\beta$ chemical shifts on protein structure determination by NMR. *J. magn. Reson.* ***B*** **106**, 92–96 (1995).
17. Grzesiek, S. & Bax, A. Measurement of amide proton exchange rates and NOEs with water in $^{13}C/^{15}N$-enriched calcineurin B. *J. biomolec. NMR* **3**, 627–638 (1993).
18. Clore, G.M., Bax, A., Omichinski, J.G. & Gronenborn, A.M. Localization of bound water in the solution structure of a complex of the erythroid transcription factor GATA-1 with DNA. *Structure* **2**, 89–94 (1994).
19. Garrett, D.S. *et al.* The impact of direct refinement against three-bond HN-CαH coupling constants on protein structure determination by NMR. *J. magn. Reson.* ***B*** **104**, 99–103 (1994).
20. Clore, G.M., Robien, M.A. & Gronenborn, A.M. Exploring the limits of precision and accuracy of protein structures determined by nuclear magnetic resonance spectroscopy. *J. molec. Biol.* **231**, 82–102 (1993).
21. Nilges, M., Clore, G.M. & Gronenborn, A.M. Determination of three-dimensional structures of proteins from interproton distance data by hybrid distance geometry-dynamical simulated annealing. *FEBS Letts* **239**, 317–324 (1989).
22. Reiher, W.E. Theoretical studies of hydrogen bonding. *Ph.D Thesis* (Harvard University, Cambridge, MA; 1985).
23. Braun, W. & Go, N. Calculation of protein conformation by proton-proton distance constraints: a new efficient algorithm. *J. molec. Biol.* **186**, 611–626 (1985).
24. Momany, F.A., Carruthers, L.M., McGuire, R.F. & Scheraga, H.A. Intermolecular potentials from crystal data III. Determination of empirical potentials and application to the packing configurations and lattice energies in crystals of hydrocarbons, carboxylic acids and amides. *J. phys. Chem.* **78**, 1595–1620 (1974).
25. Clubb, R.T., Omichinski, J.G., Sakaguchi, K., kApella, E., Gronenborn, A.M. & Clore, G.M. Backbone dynamics of the oligomerization domain of p53 determined from ^{15}N NMR relaxation measurements. *Prot. Sci.* **in the press.**
26. Laskowski, R.A., MacArthur, M.W., Moss, D.S. & Thornton, J.M. PROCHECK: a program to check the stereochemical quality of protein structures. *J. appl. Crystallogr.* **26,** 283–291 (1993).
27. Kabsch, W. & Sander, C. Dictionary of protein secondary structre: pattern recognition of hydrogen-bonded and geometrical features. *Biopolymers* **22**, 2577–2637 (1983).
28. Eisenberg, D. & MacLachlan, A.D. Solvation energy in protein folding and binding. *Nature* **319**, 199–203 (1986).
29. Chiche, L., Gregoret, L.M., Cohen, F.E. & Kollman, P.A. Protein model structure evaluation using the solvation free energy of folding. *Proc. natn. Acad. Sci. U.S.A.* **87**, 3240–3243 (1990).
30. Vuister, G.W. & Bax, A. Quantitative J correlation: a new approach for measuring homonuclear three-bond $J(H^NH^\alpha)$ couplings in ^{15}N-enriched proteins. *J. Am. chem. Soc.* **115**, 7772–7777 (1993).
31. Bax, A., Max, D. & Zax, D. Measurement of multiple-bond ^{13}C-^{13}C J couplings in a 20 kDa protein-peptide complex. *J. Am. chem. Soc.* **114**, 6923–6924 (1992).
32. Stürzbecher, W.W. *et al.* A C-terminal α-helix plus basic region motif is the major structural determinant of p53 tetramerization. *Oncogene* **7**, 1513–1523 (1992).
33. Sakamoto, H., Lewis, M.S., Kodoma, H., Appella, E. & Sakaguchi, K. Specific sequences from the carboxyl terminus of the human p53 gene product form anti-parallel tetramers in solution. *Proc. natn. Acad. Sci. U.S.A.* **91**, 8974–8978 (1994).
34. Waterman, J.L., Shenk, J.L. & Halazonetis, T.D. The dihedral symmetry of the p53 tetramerization domain mandates a conformational switch upon DNA binding. *EMBO J.* **14**, 512–519 (1995).
35. Creamer, T.P & Rose, G.D. Side-chain entropy opposes α-helix formation but rationalizes experimentally determined helix-forming propensities. *Proc. natn. Acad. Sci. U.S.A.* **89**, 5937–5941 (1992)
36. Handel, T.M., Williams, S.R. & DeGrado, W.F. Metal-ion dependent modulation of the dynamics of a designed protein. *Science* **261**, 879–885 (1993).
37. Cariello, N.F., Cui, L., Beroud, C. & Soussi, T. Database and software for the analysis of mutations in the human p53 gene. *Cancer Res.* **54**, 4454–4460 (1994).
38. Harper, E.T. & Rose, G.D. Helix stop signals in proteins and peptides: the capping box. *Biochemistry* **32**, 7605–7609 (1993).
39. Milner, J. & Medcalf, E.A. Cotranslation of activated mutant p53 with wild type drives the wild-type p53 protein into the mutant conformation. *Cell* **65**, 765–774 (1991).
40. Bargonetti, J., Reynisdottir, J., Friedman, P.N. & Prives, C. Site specific binding of wild-type p53 to cellular DNA is inhibited by SV40 T antigen and mutant p53. *Genes Develop.* **6**, 1886–1898 (1992).
41. Shaulian, E., Zauberman, A., Ginsberg, D. & Oren, M. Identification of a minimal transforming domain of p53: negative dominance through the abrogation of sequence-specific DNA binding. *Molec. cell Biol.* **12**, 5581–5592 (1992).
42. Halazonetis, T.D. & Kandil, A.N. Conformational shifts propogate from the oligomerization domain of p53 to its tetrameric DNA binding domain and restore DNA binding to select p53 mutants. *EMBO J.* **12**, 5057–5064 (1993).
43. Hainaut, P., Hall, A. & Milner, J. Analysis of p53 quaternary structure in relation to sequence specific DNA binding. *Oncogene* **9**, 299–303 (1994).
44. Ziegler, A. *et al.* Sunburn and p53 in the onset of skin cancer. *Nature* **372**, 773–776 (1994).
45. Aurora, R., Srinivasan, R. & Rose, G.D. Rules for α-helix termination by glycine. *Science* **264**, 1126–1130 (1994).
46. Soussi, T., de Fromentel, C.C. & May, P. Structural aspects of the p53 protein in relation to gene evolution. *Oncogene* **5**, 945–952.
47. Dayhoff, M.O. *Atlas of Sequence and Structure* (National Biomedical Research Foundation, Silver Spring, U.S.A.; 1969).
48. Bodenhausen, G. & Ruben, D.J. Natural abundance nitrogen-15 NMR by enhanced heteronuclear spectroscopy. *Chem. Phys Letts* **69**, 185–189 (1980).
49. Yamazaki, T. *et al.* NMR and X-ray evidence that the HIV protease catalytic aspartyl groups are protonated in the complex formed by the protease and a non-peptide cyclic urea-based inhibitor. *J. Am. chem. Soc.* **116**, 10791–10792 (1994).
50. Brünger, A.T. *X-PLOR Version 3.1 Manual* (Yale University, New Haven, CT, U.S.A.; 1992).
51. Nilges, M. A calculational strategy for the structure determination of symmetric dimers by ^1H NMR. *Proteins Struct. Funct. Genet.* **17**, 295–309 (1993).
52. Clore, G.M., Appella, E., Yamada, M., Matsushima, K. & Gronenborn, A.M. Three-dimensional structure of interelukin-8 in solution. *Biochemistry* **29**, 1689–1696 (1990).
53. Kraulis, P.J. *et al.* Determination of the three-dimensional solution structure of the C-terminal domain of cellobiohydrolase I from *Trichoderma reesei*: a study using nuclear magnetic resonance and hybrid distance geometry-dynamical simulated annealing. *Biochemistry* **28**, 7241–7257 (1989).
54. Brünger, A.T. & DeLano, W. *AVSXPLOR User Manual*, Yale University, New Haven, CT, U.S.A. (1992).
55. Carson, M. Ribbon models of macromolecules. *J. molec. Graphics* **5**, 103–106 (1987).
56. de Castro, E. & Edelstein, S. *VISP 1.0 User's Guide* (University of Geneva, Switzerland; 1992).
57. Brooks, B.R. *et al.* CHARMM: a program for macromolecular energy minimization and dynamics calculations. *J. comput. Chem.* **4**, 187–217 (1983).
58. Richards, F.M. & Kundrot, C.E. Identification of structural motifs from protein coordinate data: secondary structure and first level supersecondary structure. *Proteins Struct. Funct. Genet.* **3**, 71–84.
58. Lodi, P.J. *et al.* High-resolution structure of the β-chemokine hMIP-1β by multidimensional NMR. *Science* **263**, 1762–1767 (1994).